Size dependence of the dielectric function of silicon-supported plasmonic gold nanoparticles

Maria Losurdo,[1,*] Maria M. Giangregorio,[1] Giuseppe V. Bianco,[1] Alexandra A. Suvorova,[2] Charlie Kong,[3] Sergey Rubanov,[4] Pio Capezzuto,[1] Josef Humlicek,[5] and Giovanni Bruno[1]

[1]*Institute of Inorganic Methodologies and Plasmas (IMIP)-CNR, via Orabona 4, 70126 Bari, Italy*

[2]*Centre for Microscopy, Characterisation and Analysis, The University of Western Australia, Crawley 6009, Australia*

[3]*University of New South Wales, Sydney, New South Wales 2052, Australia*

[4]*University of Melbourne, Victoria 3052, Australia*

[5]*Masaryk University, Kotlarska 2, CZ 61137 Brno, Czech Republic*

(Received 14 July 2010; revised manuscript received 5 October 2010; published 28 October 2010)

Gold nanoparticles (NPs) are directly deposited on a Si(111) substrate by Ar sputtering to provide a semiconductor-based plasmonic platform. The Au NPs are characterized by interband transitions at energies above 2.5 eV, whose tails extend into the surface-plasmon resonance (SPR) region, hence affecting the SPR energy, amplitude, and broadening. Herein, we report the experimental evidence of the size dependence of the interband transitions for Au NPs supported on silicon and sapphire substrates by exploiting plasmonic ellipsometry. Providing the size dependence of the dielectric function of Au NPs in the extended spectral range of 190–1700 nm, and discussing the interconnection between the SPR and the interband transitions, this study as a whole represents a step ahead in the perspective of a better understanding of nanosize effect on optical properties and standardization of nanoparticles dielectric functions to rely on more accurate modeling of NPs behavior.

DOI: 10.1103/PhysRevB.82.155451 PACS number(s): 78.20.Ci, 81.16.−c, 78.67.Bf

I. INTRODUCTION

Recently, the interest in the preparation, characterization, and exploitation of the surface-plasmon resonance (SPR) of metal nanoparticles, and specifically of gold (Au) nanoparticles (NPs), has grown exponentially.[1,2] This interest has been driven both by technological applications spanning from biomedicine,[3,2] sensing and biosensing[3] to catalysis and to nanophotonics[4,5] and by the basic physics involved in the size-dependent structural, optical and electronic properties, which can be tailored to be suitable for device applications by the artificially designed geometries that enable the needed functionality for the nanostructures.[6–9] Therefore, optical properties of Au NPs are still widely investigated.[10–12] Typically, optical investigations focus mainly on the SPR of Au NPs, and its dependence on extrinsic effects such as NPs size and shape factor,[13] the dielectric properties of the surrounding medium,[14] and the internanoparticles coupling interactions.[15–17]

Indeed, the dielectric function, $\varepsilon(\omega)$, of metals, and of Au as well, is characterized by the Drude free-electron component, $\varepsilon_{\mathrm{Drude}}(\omega)$, and by the interband transitions component, $\varepsilon_{\mathrm{inter}}(\omega)$, involving transitions from *d levels* to an empty state above the Fermi level ($d \rightarrow E_F$), i.e.,

$$\varepsilon(\omega) = \varepsilon_{\mathrm{Drude}}(\omega) + \varepsilon_{\mathrm{inter}}(\omega).$$

Although the impact of lattice defects within the nanoparticles as well as nonhomogeneous distribution of size and shape of nanoparticles have to be also considered, the predominant size effects on the SPR mainly due to the Drude free electrons, $\varepsilon_{\mathrm{Drude}}(\omega)$, are extensively investigated. Indeed, the bound electrons contribution to the dielectric function also plays an important role in determining plasmon resonance wavelength and broadening.

Nevertheless, there are two aspects that are still critical and interesting from both fundamental and technological points of views worthy of being duly investigated, which are the intrinsic size dependence of the dielectric function of the metal nanoparticles itself and the interconnection of the SPR to the Au NPs interband transition contribution, $\varepsilon_{\mathrm{inter}}(\omega)$; the latter accounts for the response of $5d$ electrons to a $6sp$ conduction band, which is also size dependent. A rigorous extension of the Drude formula for optical response of metals was developed by Bassani and Parravicini[18] where contributions from both Drude and interband transitions develop size dependencies for sufficiently small nanoparticles.

As concern gold specifically, the extinction coefficient spectrum of bulk gold, which reflects its energy band structure (see Fig. 1), is characterized by two main structures that correspond to interband transitions: the edge at 496 nm (2.5 eV) and the first peak at ~400 nm (around 3 eV) are due to transitions from the uppermost $5d$-valence electron bands (band 5) to states in the s, p bands (band 6) just above the Fermi level,[19] indicated also as $L_3 \rightarrow L_2$ transition.[20] The peak at ~300 nm (around 4 eV) is a composite structure involving transitions from lower-lying d bands (3 and 4) to band 6 and transitions from s, p states in band 6 across the $L_6^- \rightarrow L_6^+$ gap to s-, p-like states in band 7, indicated also as $L_2' \rightarrow L_1$.[19–21]

Modifications to the lattice structure due to size effects and surface atoms, the high surface-to-volume ratio of nanoparticles, and any quantum confinement of charged carriers change the electronic structure and, hence, the dielectric function of Au nanoparticles also in the interband transition region.[22] In particular, the relatively flat upper d bands are distorted by size effects,[23–25] therefore rendering the $\varepsilon_{\mathrm{inter}}(\omega)$ of Au NPs also size dependent.

The interband transitions, through dynamical screening effects and via nonradiative decay into electron-hole excita-

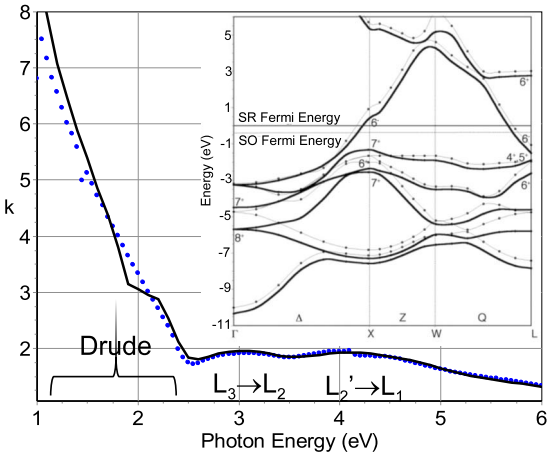

FIG. 1. (Color online) Spectra of the extinction coefficient, k, for an experimental sputtered 100-nm-thick gold film (dots) and from literature (line) (Ref. 44), with indicated the main intraband and interband electron transitions. The inset shows the gold band diagram sketch from Ref. 21. The thin and bold lines refer to the scalar-relativistic (SR) and the fully relativistic (scalar and spin-orbit effects) ground-state calculations, respectively.

tions, also influence the wavelength, amplitude, and broadening of the plasmon resonance.[26–28] This is especially true for nanosized Au clusters, which have a tail of the interband threshold extending to 1.8 eV,[29] thus affecting the wavelength/energy region where the Au NPs plasmon resonance occurs and causing asymmetric SPR peaks. Kreibig[30] first detected the size dependence of bound electrons for gold particles and found that, as the particle size becomes smaller than 40 Å, the onset of interband transition shifts slightly to the lower energy region. However, his study was limited by the spectral range that was below 4 eV, missing information and details on the interband transitions. A size effect on the slope of the onset of interband absorption as a shift to lower energy has been reported by Yamaguchi for Au (Ref. 23) and Ag (Ref. 31) nanoparticles as well, thus affecting SPR. Indeed, Pinchuk[26,27] showed that intrinsic size effect on the Au NPs dielectric function cannot absolutely be neglected for Au nanoparticles sizes below 30 nm. Indeed, in addition to quantum confinement effects, it should also be considered that surface atoms have a reduced coordination number than atoms in the bulk; therefore, in nanoparticles, which are characterized by a high surface-to-volume ratio, the reduced coordination number of surface atoms assumed noticeable importance. This is because the reduced coordination number of surface atoms, which depends on nanoparticles size, affects the density of states and, consequently, the interband transitions and related absorption. Furthermore, recently it has also been reported that effects of tensile and compressive strain induce modifications to both the bound (interband) and free (intraband) electron dielectric functions, and that those effects and modifications of dielectric function are important also for particle as large as 100 nm.[32]

Despite these arguments, the size effect on the interband transitions has not yet duly experimentally been evaluated and considered for Au nanoparticles. This is also important for some applications since photothermal efficiency due to the interband excitation can also change depending on nanoparticles size and this knowledge is important for managing electron heat capacity during nanoparticles photoexcitation depending on the excitation laser energy.[33]

Therefore, it is important to establish the dependence of the dielectric function also in the interband transition region of Au, as well as, other plasmonic metals, in a broad range, for an appropriate modeling and rationalization of plasmonic properties of metal NPs, rather than using the dielectric function of the corresponding bulk metal. Contrariwise, in most of the studies, the contribution of free electrons to the dielectric function is modified according to particle size, while the contribution of bound electrons is assumed to be independent of size.

Furthermore, most of the previous theoretical and experimental investigations referred to nanoparticles of various sizes and shapes embedded in an isotropic medium (e.g., dielectric SiO_2 or in a solution). With respect to this, it is also important to have a surface-free nanoparticle without surfactants, stabilizing ligands and dispersing matrix, which, not only affect the SPR peak, but might also suppress the interband absorption or the size-induced changes in the interband absorption.[34–36]

Very few studies reported about nanoparticles supported on semiconductor substrates. In this case the presence of a substrate introduces anisotropy in the refractive index of the media surrounding the nanoparticles, as well as in the nanoparticles geometry, which are no longer spherical, but they become prolate or oblate spheroids. For supported nanoparticles, the contact area between the substrate and the metal nanoparticles is an additional parameter also affecting the plasmon resonance together with the substrate polarizability.[37–39] A very recent paper from Vernon *et al.*[40] has demonstrated the influence of the particle-substrate interaction on the SPR. Furthermore, the details of the nanoparticles/substrate interface are relevant and crucial beyond the influence of the media dielectric function.

Herein, we experimentally demonstrate the impact of Au nanoparticles size on the high-energy interband transitions, which in turn affect the surface-plasmon resonance. The spectral dependence of the dielectric function of Au nanoparticles with a diameter in the range 14–60 nm supported on Si(111) and c-axis (0001)-oriented sapphire [α-Al_2O_3 (0001)] substrates is determined in the broad spectral range 0.75–6.5 eV (180–1700 nm). To demonstrate the validity of the present results, the approach is twofold: (1) a careful investigation of the Au NPs/Si interface has been carried out since it is considerably challenging extracting from the ellipsometric analysis the positions of interband contributions to the dielectric function of Au NPs. The challenging analysis stems from the presence of an interface layer between the Au NPs and the Si substrate and from the prominence of the Si interband critical points[41] at ~3.4 and 4.3 eV overlapping with the positions of the Au bands at ~3.0 and ~4.0 eV. Defining the interface properties by corroborating techniques allows reducing the number of fit parameters in the ellipsometric analysis. (2) An inert substrate that does not have any features (i.e., $k=0$ in all the investigated spectral range) interfering with the Au interband transitions, such as sapphire, has also been used. Therefore, this work extends and consid-

ers the effect of nanosize to the interband transitions of semiconductor-supported Au nanoparticles.

II. EXPERIMENTAL

Au nanoparticles were deposited directly on Si (111) and α-Al_2O_3 (0001) substrates by using a radio-frequency (rf), 13.5 MHz Ar plasma to sputter a high-purity Au target.[42] The rf power, pressure, Ar flow rate were fixed at 14 W, 0.3 Torr, and 10 SCCM, respectively. The sputtering time, i.e., the Au monolayer (ML) and the substrate temperature (60 and 400 °C) were varied to obtain Au nanoparticles of different size.

Two resonances can be excited in supported gold spheroids nanoparticles: a high-wavelength (low-energy) longitudinal mode that corresponds to collective oscillations along the major axis parallel and a low-wavelength (transverse) mode in the direction perpendicular to the surface (minor axis of the spheroid). For the present NPs size and shape, the low-wavelength Au NPs transverse SPR mode is damped due to the nonradiative decay into electron-hole excitations of the nearby interband transitions and, therefore, cannot be seen in the optical spectra.

Optical characterization was performed exploiting spectroscopic ellipsometry.[43] Spectroscopic ellipsometry measurements of the pseudoextinction coefficient, $\langle k \rangle$, were performed in the range 190–1700 nm (0.75–6.5 eV) with a phase-modulated spectroscopic ellipsometer (UVISEL-Jobin Yvon) at an incidence angle of 70°. The spectral dependence of the extinction coefficient, k, of Au NPs was derived from the measured ellipsometric spectra by their analysis with a two-layer model (substrate/interface/Au NPs/air) built on the basis of complimentary information obtained by high-resolution cross-sectional transmission electron microscopy (HR-TEM) and atomic force microscopy (AFM).

The compositional and structural variations in the samples were studied using a combination of HR electron microscopy (HREM) and energy-filtered TEM (EFTEM) using a JEOL 3000F field-emission gun TEM equipped with a Gatan image filter and digital camera. The specimen for TEM analysis was prepared with an FEI Nova Nanolab 200 Dualbeam focused ion beam. To prevent the top surface from ion-beam damage, a two-step *in situ* Pt deposition was carried out on the region of interest. At first, a Pt strip of $20 \times 2 \times 0.1$ μm^3 was slowly deposited with the electron beam operating at 30 kV and 0.15 nA. Then a thick reinforce strip of Pt deposition of $20 \times 2 \times 1$ μm^3 was toped up by faster ion-beam deposition operating at 30 kV and 0.3 nA. This process would not only protect the beam sensitive specimen from the damage of ion beam during all the milling/imaging steps but also prevent any possible damage which might be induced during the direct ion-beam Pt-deposition process. The chemical information was visualized by generating EFTEM images of constituent elements. To observe the elemental distribution within a Au/interface/Si stack, EFTEM images were acquired for the silicon $L_{2,3}$ edge, oxygen K edge, and gold $O_{2,3}$ edge using the standard three window method and the optimum elemental mapping parameters calculated by use of a reference spectrum. The thickness of the oxide layers was

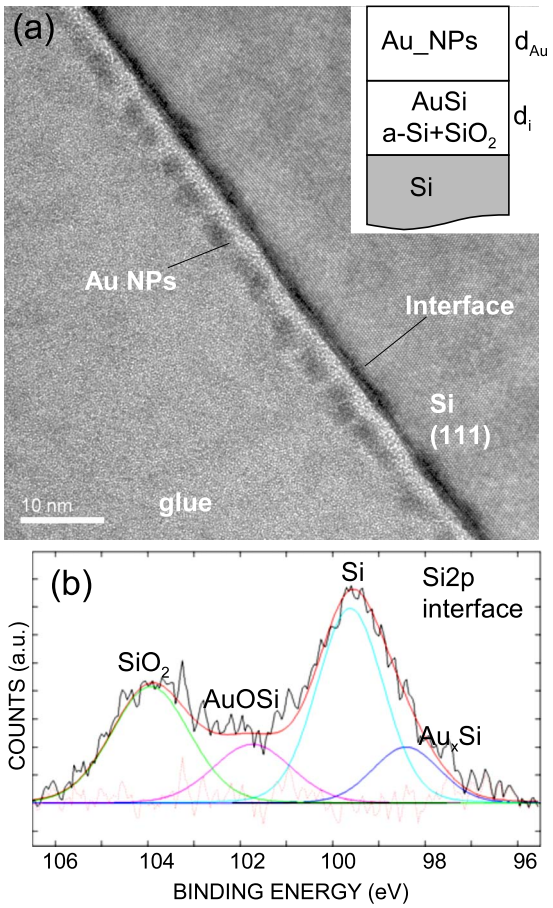

FIG. 2. (Color online) (a) HR-TEM image of Au NPs sputtered on Si at room temperature showing the Au-Si interface layer. (b) XPS spectrum of the Si $2p$ photoelectron core level showing the presence of SiO_2 and gold silicide AuSi at the interface. The inset in (a) shows the model used for fitting ellipsometric spectra and built on the basis of the TEM and XPS input data.

estimated from a line profile across the layers using the full width at half maximum of the profile peak and was correlated with the HREM measurements.

The surface-plasmon resonance and the interband transitions of the Au-nanoparticle ensemble were parametrized by a combination of three-Lorentzian oscillators

$$N^2 = (n + ik)^2 = \varepsilon = \varepsilon_1 + i\varepsilon_2 = \varepsilon_\infty + \sum_j \frac{A_j \omega_j^2}{\omega_j^2 - \omega^2 - i\gamma_j \omega},$$

where ε_∞ is the high-frequency dielectric constant, ω_j, γ_j, and A_j are the frequency, width and strength of the j oscillator. The first oscillator describes the SPR, whose wavelength, amplitude, and broadening, γ_{SPR}, can be determined. Interestingly, from the plasmon peak broadening, the plasmon dephasing time $T_2 = 2\hbar / \gamma_{SPR}$ can be calculated as a function of Au NPs size. The second and the third higher energy oscillators describe the $L_3 \rightarrow L_2$ and $L_2' \rightarrow L_1$ interband transitions.

The chemical species analysis was also run by x-ray photoelectron spectroscopy (XPS) using a Kratos Analytical axis spectrometer equipped with a monochromatic Al $K\alpha$ x-ray

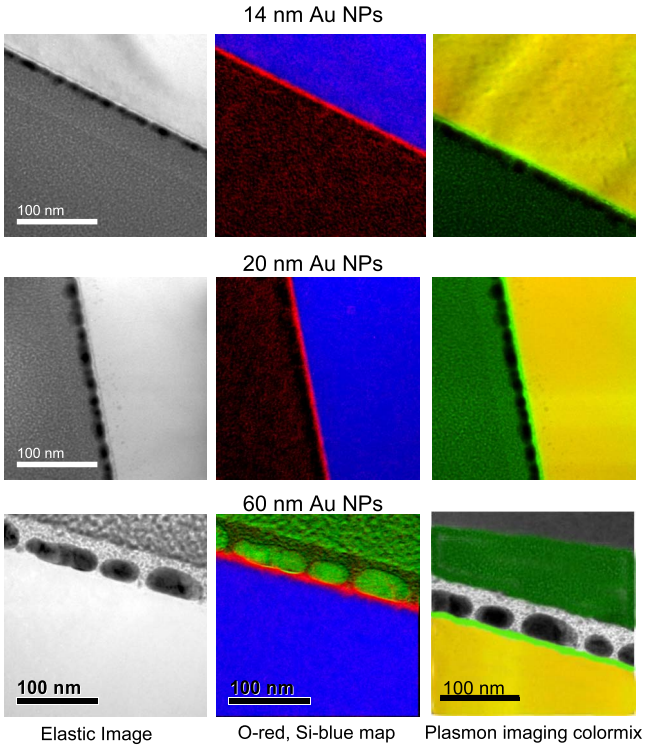

FIG. 3. (Color online) Elastic TEM image, chemical elements maps (O—red, Si—blue), and Si (17 eV) (yellow) SiO_2 (23 eV) plasmon color mixing for gold nanoparticles of average diameter of (a) 14 nm, (b) 20 nm, and (c) 60 nm.

source. Spectral calibration was determined by setting the main C 1*s* component at 284.5 eV and the Au $4f_{7/2}$ line at 84.0 eV. The main core photoelectron levels investigated were Si 2*p*, C 1*s*, O 1*s* and Au 4*f*. Photoelectron core-levels spectra were acquired with pass energy of 20 eV

The nanoparticles were imaged by AFM performed in the intermittent-contact mode using an AutoProbe CP Thermomicroscope. A high aspect ratio probe-supersharp tip with a radius of curvature of 2 nm (ESP Series Probes-VEECO) was used.

III. RESULTS AND DISCUSSION

Figure 2(a) shows the HR-TEM image of Au NPs sputtered on Si at 60 °C, which put in evidence the formation of an extended, amorphous, and rough alloyed interface layer between the Au NPs and the Si substrate. The interface layer is a mixture of AuSi and SiO_2, as confirmed by EFTEM (see also Fig. 3) and by XPS spectrum of the Si 2*p* photoelectron peak shown in Fig. 2(b). The thickness of the interface layer was obtained by HR-TEM (see Figs. 3 and 4) and the ratio of the SiO_2/AuSi was determined from XPS and both were used as input and fixed in the ellipsometric analysis. In particular, the Si 2*p* core level in Fig. 2(b) shows main peak component at a binding energy (BE) of 99.7 eV due to the Si substrate and at BE of 103.8 eV due to the interface SiO_2, together with additional peaks at BE of 98.2 and 101.5 eV, which are indicative of interface intermixing, i.e., gold silicide AuSi and its oxide. Standard dielectric functions of

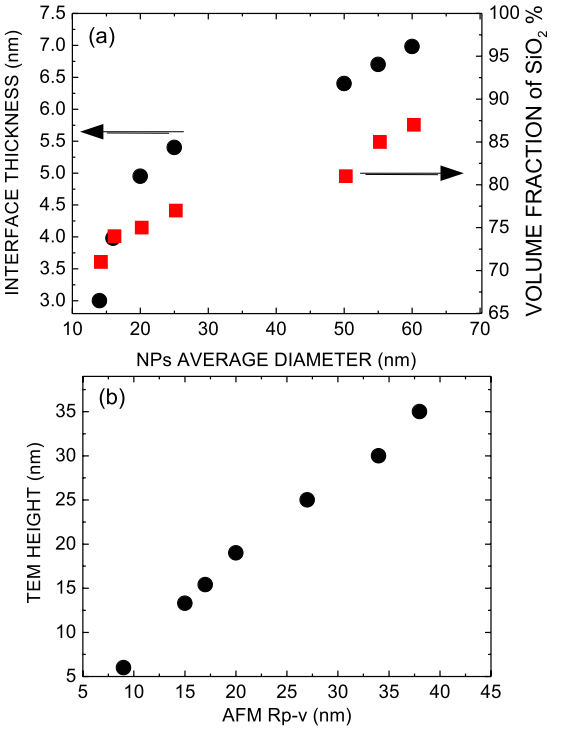

FIG. 4. (Color online) (a) The interface thickness, d_I, derived by the HR-TEM analysis as a function of Au deposited monolayers (left axis); the SiO_2 volume fraction (in addition to AuSi) of the interface layer (right axis). (b) Correlation between the height of the Au NPs layers as determined by TEM cross-section analysis and the peak-to-valley height, *Rp-v*, from AFM measurements.

c-Si(111),[41] SiO_2,[44] and the AuSi alloy[45] were applied in the modeling of the interface using the Bruggemann effective-medium approximation (BEMA) [see inset of Fig. 2(a)].[46] As for the Si(111) substrate dielectric function, it was checked that there is no disparity between the position of the interband CPs of Si from Ref. 41 and those for the present sub-

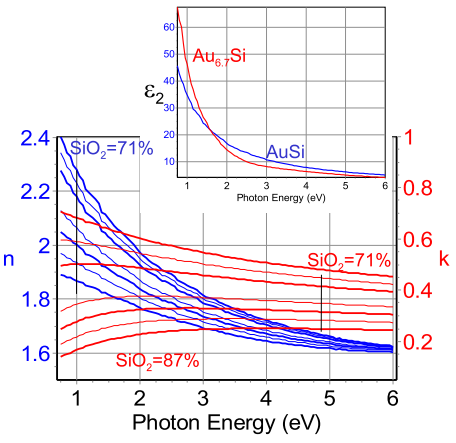

FIG. 5. (Color online) Spectral dependence of the composite (BEMA SiO_2+AuSi) refractive index, *n*, and extinction coefficient, *k*, from 71% SiO_2+29% AuSi till 87% SiO_2+13% AuSi, with an increment of 2% SiO_2. The inset shows the imaginary part, ε_2, of the dielectric function of the AuSi and $Au_{6.7}Si$ silicides from Ref. 45.

TABLE I. Energy position of the SPR and interband transitions assuming two extreme silicide stoichiometries in the BEMA interface layer (see Fig. 4), for three representative nanoparticles sizes.

	14 nm			20 nm			60 nm		
	SPR	$L_3 \rightarrow L_2$	$L_2' \rightarrow L_1$	SPR	$L_3 \rightarrow L_2$	$L_2' \rightarrow L_1$	SPR	$L_3 \rightarrow L_2$	$L_2' \rightarrow L_1$
AuSi	2.159 ± 0.016	3.630 ± 0.035	4.315 ± 0.036	1.945 ± 0.019	3.320 ± 0.008	4.134 ± 0.013	1.868 ± 0.005	3.085 ± 0.019	4.010 ± 0.013
$Au_{6.7}Si$	2.162 ± 0.019	3.641 ± 0.055	4.313 ± 0.038	2.041 ± 0.027	3.322 ± 0.007	4.138 ± 0.014	1.885 ± 0.007	3.083 ± 0.021	4.014 ± 0.015

strate, therefore no errors due to uncertainty in the substrate peak position manifests in the Lorentzian band positions of Au NPs.

For the interface layer, it has to be considered that, although the SiO_2 layer initially is minimized by the native oxide removal by the fluoridric acid wet etching of the Si substrate before loading it into the reactor, it may stem from the air-exposure and postdeposition oxidation of the gold-silicide interface, since gold silicides quickly oxidize.[47] The HR-TEM analysis was run on all samples in this work, in order to reduce all possible indetermination due to interface in the ellipsometric analysis, where the only fit parameters where the oscillators parameters describing the gold nanoparticles layer.

Figure 3 shows the elastic image, the chemical element color map O—red and Si—blue, and the plasmon imaging colormix (Si-plasmon 17 eV—yellow and SiO_2 plasmon 23 eV imaging) of three representative samples [(a), (c), and (g), along the diagonal in Fig. 6] obtained under different deposition conditions to attest the effect of sputtering time and temperature on the interface layer and on the nanoparticles geometry as well. The chemical element maps mainly shows that the oxygen is localized at the interface between the substrate and the gold NPs, whereas the Si and SiO_2 plasmon colormix map indicates the homogeneous interfacial intermixing of Si and SiO_2, providing a visual evidence that the interface is mainly SiO_2; furthermore, the sharp color contrast is indicative of a very low interface roughness especially for samples deposited at the low temperature of 60 °C.

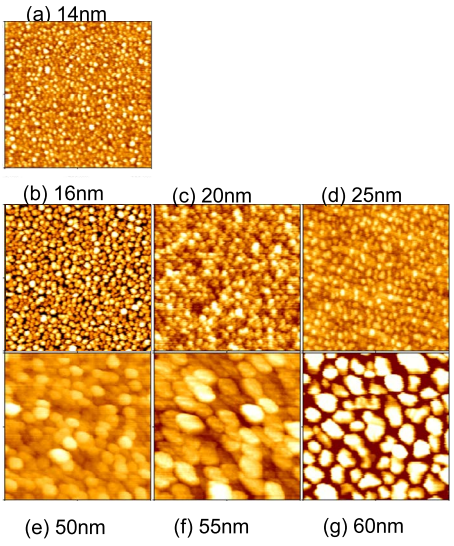

FIG. 6. (Color online) 500 nm × 500 nm AFM images of Au NPs with different average diameter sputtered at [(a)–(d)] 60 °C and at [(e)–(g)] 400 °C.

The interface thickness, d_I, is reported in Fig. 4(a) as a function of the average lateral size (diameter) of the nanoparticles estimated by the TEM cross sections and by the AFM plain views (the latter run statistically on various points of the samples) and those values have been fixed in the ellipsometry modeling. It is found that the interface thickness increases with sputtering time and with surface temperature, and its thickness cannot be neglected when compared to the average particle height as estimated by TEM cross sections [see Figs. 4(a) and 4(b)]. Furthermore, from the compositional point of view, Fig. 4(a) also shows that the interface enriches in SiO_2 with the increase in sputtering time and temperature, i.e., with the increase in NPs' size. A deeper insight into the dielectric properties assigned to the interface depending on its composition as from Fig. 4(a), is

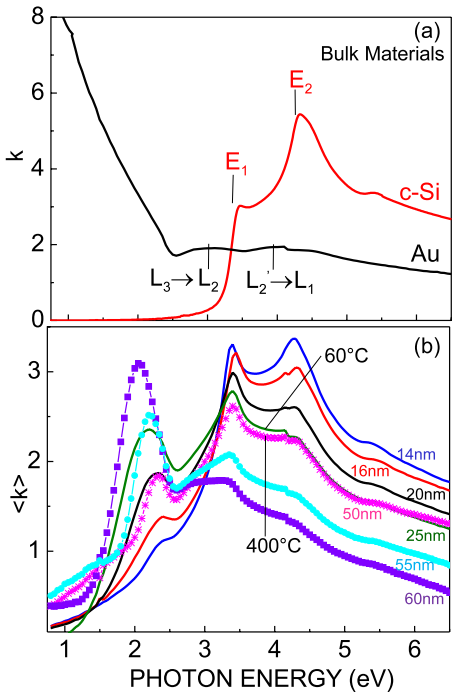

FIG. 7. (Color online) (a) Ellipsometric spectra of the extinction coefficient, k, of bulk c-Si (from Ref. 43) and Au (from Ref. 44). (b) Pseudoextinction coefficient, $\langle k \rangle$, of the NPs ensembles of various diameters as determined by AFM deposited at 60 °C [(a)–(d); continuous lines] and 400 °C [(e)–(g); symbols]. The average diameters are from TEM cross sections and AFM line profiles scanned in various points of each image). The main interband transitions for both c-Si and Au are indicated.

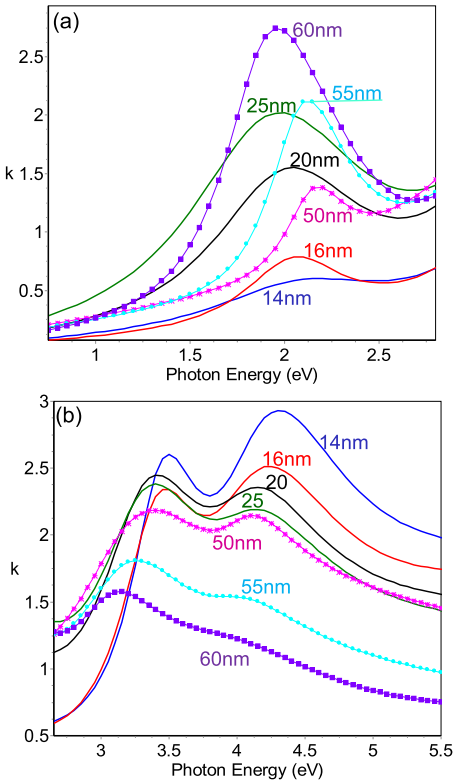

FIG. 8. (Color online) Spectra of (a) the SPR peak and (b) of the interband transitions spectral regions of the ensembles of Au NPs with different sizes. Lines refer to NPs deposited at 60 °C; symbols refer to NPs deposited at 400 °C.

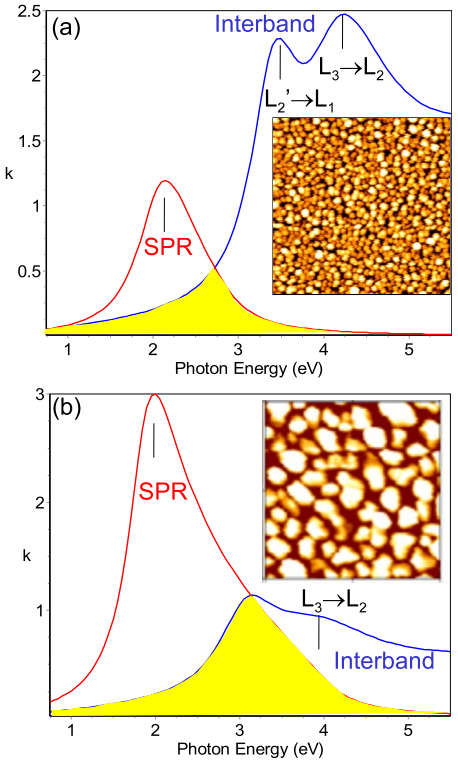

FIG. 9. (Color online) Contributions of the SPR peak (red line) and of the interband transitions (blue line) for two NPs samples with a NPs average size of (a) 16 nm (deposited at 60 °C) and (b) 60 nm (deposited at 400 °C). The overlapping region between the SPR and interband contributions, which is size dependent, is also shown as yellow area. In the inset the corresponding 500 nm ×500 nm AFM images are also shown.

provided in Fig. 5 that shows the spectral dependence of the composite (BEMA SiO_2+AuSi) refractive index, n, and extinction coefficient, k. It is worth noting that with the change in the relative fraction of SiO_2 and AuSi there is a monotone trend in the properties of the interface without characteristic features in the region >3 eV which might interfere with the position of the interband gold transition. Furthermore, the inset shows the dielectric properties of the two extreme AuSi and $Au_{6.7}Si$ silicides stoichiometry reported so far in literature.[45] It can also be noted that although there is an inflection point depending on the Au fraction, almost flat profiles characterize the region of interest for the gold interband critical points; hence, a possible not enough accurate determination of the silicide interface stoichiometry does not affect the position of Au interband critical points, as will be demonstrated in the below (see Table I).

Figure 6 shows the AFM images of Au NPs with increasing size. By the analysis of AFM images in terms of line profiles and histograms, average values for Au NPs diameters and the peak-valley parameter, Rp-v, (the highest data point minus the lowest point in the scan area, Rp-v=z_{max} −z_{min}) were determined. By a comparison of the TEM and AFM data, it was found that the Rp-v by AFM correlates to the thickness of the Au NPs ensemble layer determined by TEM as shown in Fig. 4(b). Therefore, the Au NPs layer thickness in the ellipsometric analysis has been fixed to the average height of NPs as determined by TEM cross sections. This further contributes to improve accuracy of ellipsometry fitting results.

The corresponding ellipsometric spectra of the pseudoextinction coefficient, $\langle k \rangle$, of the NPs ensembles supported on Si are shown in Fig. 7. For comparison the bulk dielectric functions of c-Si (Ref. 51) and Au (Ref. 48) are also shown. The $\langle k \rangle$ spectra are characterized by the presence of the SPR characteristic of the Au NPs with the amplitude increasing and the position redshifting with the increase in Au MLs and NPs size. For photon energies above 3 eV, the characteristic critical points E_1 and E_2 of c-Si (Ref. 41) predominate in the spectra of Fig. 7 for Au NPs on Si, whose amplitude decreases with the increase in the deposited Au MLs. This spectral region is also sensitive to the interband absorption of Au, as shown in Fig. 7(a). The continuous lines in Fig. 7(b) correspond to the ellipsometric fit using the two-layer model (sketched in the inset of Fig. 2) that includes an interface layer[49] with thickness d_i, which consists of a mixture of AuSi alloy and SiO_2 (detected by XPS) and a top layer representing the Au NPs ensemble. The oscillator parameters describing the optical function of the Au NPs ensemble were the fit parameters. The spectra derived in the broad range from 0.75 to 6.5 eV (190–1700 nm) of the extinction coefficient, k, of the ensembles of Au NPs with different sizes are reported in Fig. 8. The spectra of the extinction coefficient of Au NPs are characterized by the presence of three main peaks, i.e., the SPR peak, whose details are shown in Fig. 8(a) and the interband transitions, whose spectral region is detailed in Fig. 8(b).

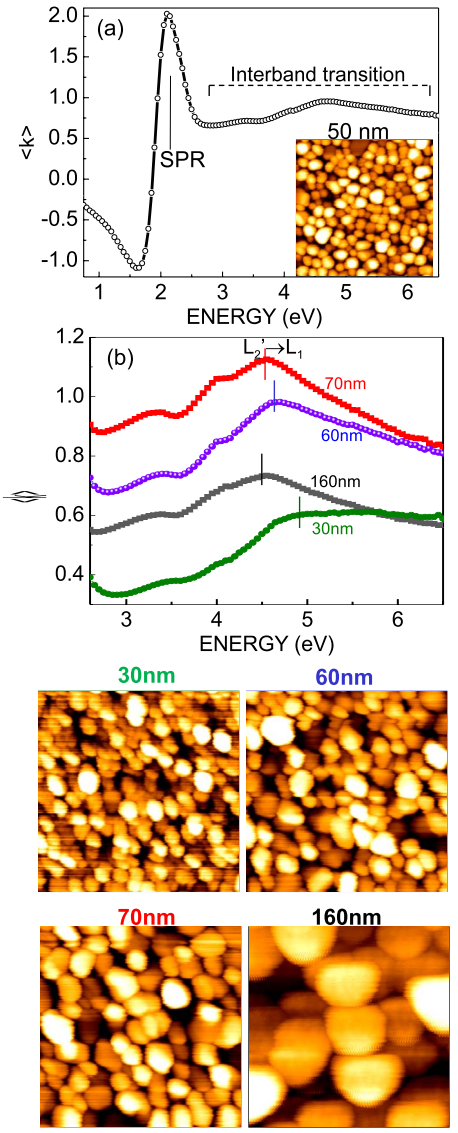

FIG. 10. (Color online) (a) Ellipsometric spectra of the pseudoextinction coefficient, $\langle k \rangle$, for Au NPs with an average diameter of 50 nm deposited on α-$Al_2O_3(0001)$ (which has $k=0$ in all the investigated experimental range; hence the spectral features are due to the Au NPs). The inset shows the corresponding 500 nm $\times$500 nm AFM image. (b) Pseudoextinction coefficient, $\langle k \rangle$, spectra enlarged in the interband transitions spectral region and corresponding 500 nm$\times$500 nm AFM images for gold nanoparticles of different size deposited on α-$Al_2O_3(0001)$.

The main result from Fig. 8 is that not only the SPR but also the interband transitions are size dependent, clearly suggesting that size effects on interband transitions are important and may persist to surprisingly size >50 nm. Furthermore, some representative data in Table I indicate that the shift observed for the interband transition is not due to any indetermination in the stoichiometry interface, which rather, indeed, may affect more the SPR energy. The interconnection between the SPR and the interband region, which is responsible of the nonradiative decay of the plasmon, is shown in Fig. 9 also depending on NPs' size.

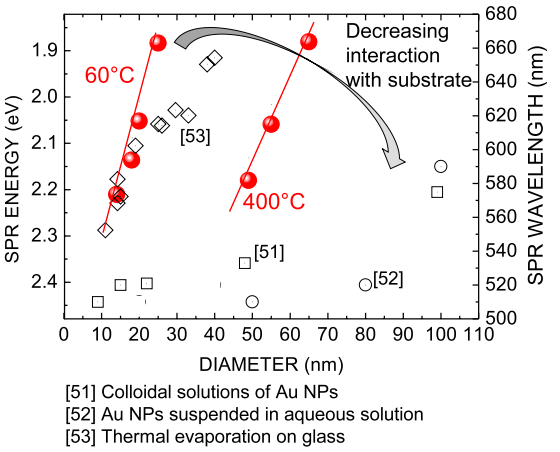

FIG. 11. (Color online) Dependence of the SPR wavelength on NPs size. The red—full spheres refer to data from the present work with two sets of data for the 60 and 400 °C deposited NPs. For comparison, data from Refs. 51–53 are also shown (black empty symbols).

In order to demonstrate that the size dependence of the Au interband critical points is not an artifact of the model analysis and/or of the interference with the E_1 and E_2 Si CPs, Au NPs have also been deposited on transparent ($k=0$) sapphire substrate. The experimental measured spectra (no fit model analysis applied) are shown in Fig. 10 with the corresponding AFM images. Clearly a redshift with the size increase in NPs is observed especially for the $L_2' \rightarrow L_1$ Au interband transition.

The SPR wavelength dependence on NPs size is shown in Fig. 11. The present experimental results (red spheres) for NPs supported on Si(111) are compared with data reported in literature for colloidal spherical Au NPs,[50,51] for Au NPs suspended in aqueous solution,[52] and for Au NPs supported on glass.[53–55] Interestingly, the SPR of Au NPs supported on substrates redshift more than spherical NPs of the same size dispersed in solutions, and the slope of the variation is higher. This can be understood in the frame of the theory recently proposed by Vernon,[40] i.e., the electric fields from the surface charges in NPs polarize the substrate and induce additional surface charges at the interface between the substrate and the surrounding medium. As a result, the interaction of NP with the substrate is also NP size and shape dependent. Specifically, the interaction with the substrate decreases with the nanoparticles elongation parallel to the substrate[40] (as a consequence of the localization of the charge only at the ends of the ellipsoidal. Therefore, the lower the interaction with the substrate the lower the redshift tending to the trend for isolated nanoparticles.

Similarly, Fig. 12 shows the dependence of the wavelength of the interband Au transitions on NPs average diameter. The interband transitions also redshift with the increase in particle size, approaching the values characteristic of bulk gold.

Since the dephasing time T_2, i.e., the time during which the oscillating electrons lose their phase coherence, is related to the homogeneous plasmon absorption bandwidth, the ellipsometric determination of the broadening of the Lorentz-

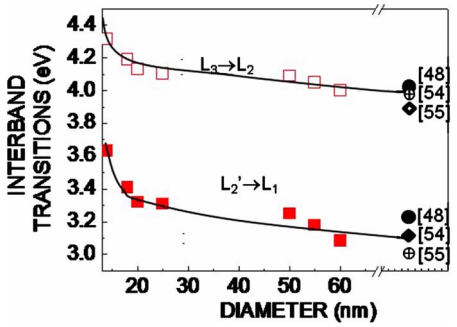

FIG. 12. (Color online) Dependence of the wavelength of the interband Au transitions on NPs average diameter from data in Fig. 8.

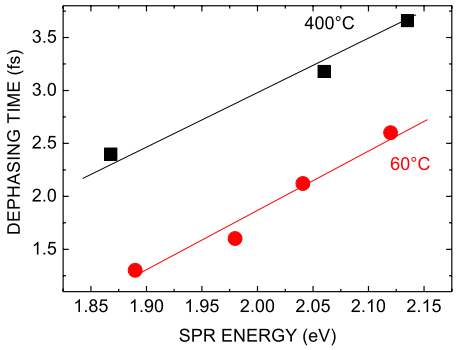

FIG. 13. (Color online) Dephasing time calculated from the SPR broadening for the various ensembles on NPs of various size deposited at low (60 °C) and high (400 °C) temperatures vs the resonance energy.

ian oscillator representing the SPR resulted in the plasmon dephasing for the various samples, which is reported in Fig. 13. As shown in the figure, the plasmon dephasing time depends on the size, decreasing with increasing the redshift.[56] For Au NPs in the range 14–60 nm, a dephasing time in the range 1.3–3.7 fs, which is consistent with previously reported values,[57] has been determined. The reduced dephasing time and, hence, plasmon decay into interband excitation for the smaller NPs deposited at lower temperature can be explained by the lower overlapping of interband states (see Fig. 11) and blueshifted interband absorption [see Fig. 8(b)].

IV. CONCLUSIONS

In conclusion, we have experimentally determined the size dependence of the dielectric function of Au nanoparticles supported on Si and sapphire substrates. It is also shown the interconnection between plasmon absorption and interband transitions for substrate-supported Au NPs.

All the factors including the interface reactivity of Au nanoparticles and silicon substrates are considered in the analysis, which includes a critical discussion of the importance of the interface in building a reliable optical model to derive properties of Au nanoparticles. Finally, we have demonstrated intrinsic size effects in the dielectric function of Au NPs also in the interband region persisting to surprisingly large size. Therefore, caution is advisable along the analysis of plasmon polaritons effects when choosing the material dielectric function to describe the nanoparticles.

ACKNOWLEDGMENTS

The authors acknowledge Alberto Sacchetti at IMIP-CNR for the technical assistance in growing samples. This work has been supported by the European Community's Seventh Framework Programme under the project NanoCharM (Grant No. NMP3-CA-2007-218570).

*Corresponding author. FAX: +39-0805443562; maria.losurdo@ba.imip.cnr.it

[1] G. H. Chan, J. Zhao, E. M. Hicks, G. C. Schatz, and R. P. Van Duyne, Nano Lett. **7**, 1947 (2007).
[2] I. H. El-Sayed, X. Huang, and M. A. El-Sayed, Nano Lett. **5**, 829 (2005).
[3] A. P. Alivisatos, K. P. Johnsson, X. Peng, T. E. Wilson, C. J. Loweth, and M. P. Bruchez, Jr., and P. G. Schultz, Nature (London) **382**, 609 (1996).
[4] S. A. Maier, P. G. Kik, H. A. Atwater, S. Meltzer, E. Harel, B. E. Koel, and A. A. G. Requicha, Nature Mater. **2**, 229 (2003).
[5] F. Seker, P. R. L. Malenfant, M. Larsen, A. Alizadeh, K. Conway, A. M. Kulkarni, G. Goddard, and R. Garaas, Adv. Mater. **17**, 1941 (2005).
[6] C. Tserkezis, N. Papanikolaou, E. Almpanis, and N. Stefanou, Phys. Rev. B **80**, 125124 (2009).
[7] Y. Xia and N. Halas, MRS Bull. **30**, 338 (2005).
[8] K. Koga, T. Ikeshoji, and K. Sugawaral, Phys. Rev. Lett. **92**, 115507 (2004).
[9] P. M. Paulus, A. Goossens, R. C. Thiel, A. M. van der Kraan, G. Schmid, and L. J. de Jongh, Phys. Rev. B **64**, 205418 (2001).
[10] P. K. Jain, X. Huang, I. H. El-Sayed, and M. A. El-Sayed, Plasmonics **2**, 107 (2007).
[11] O. L. Muskens, P. Billaud, M. Broyer, N. Del Fatti, and F. Vallee, Phys. Rev. B **78**, 205410 (2008).
[12] P. K. Jain, S. Eustis, and M. A. El-Sayed, J. Phys. Chem. B **110**, 18243 (2006).
[13] K. L. Kelly, E. Coronado, L. L. Zhao, and G. C. Schatz, J. Phys. Chem. B **107**, 668 (2003).
[14] S. Underwood and P. Mulvaney, Langmuir **10**, 3427 (1994).
[15] W. Rechberger, A. Hohenau, A. Leitner, J. R. Krenn, B. Lamprecht, and F. R. Aussenegg, Opt. Commun. **220**, 137 (2003).
[16] P. K. Jain, W. Qian, and M. A. El-Sayed, J. Phys. Chem. B **110**, 136 (2006).
[17] J. J. Storhoff, A. A. Lazarides, R. C. Mucic, C. A. Mirkin, R. L. Letsinger, and G. C. Schatz, J. Am. Chem. Soc. **122**, 4640 (2000).
[18] F. Bassani and G. Pastori Parravicini, *Electronic States and Optical Transitions in Solids* (Pergamon, New York, 1975).
[19] R. Lasser and N. V. Smith, Solid State Commun. **37**, 507 (1981).
[20] G. B. Irani, T. Huen, and F. Wooten, Phys. Rev. B **6**, 2904 (1972).

[21] R. Romaniello and P. L. de Boeij, J. Chem. Phys. **122**, 164303 (2005).
[22] B. Balamurugan and T. Maruyama, Appl. Phys. Lett. **87**, 143105 (2005).
[23] T. Yamaguchi, M. Takiguchi, S. Fujioka, H. Takahashi, and E. Anno, Surf. Sci. **138**, 449 (1984).
[24] M. G. Mason and R. C. Baetzold, J. Chem. Phys. **64**, 271 (1976).
[25] H. Roulet, J. M. Mariot, G. Dufour, and C. F. Hague, J. Phys. F: Met. Phys. **10**, 1025 (1980).
[26] A. Pinchuk, U. Kreibig, and A. Hilger, Surf. Sci. **557**, 269 (2004).
[27] A. Pinchuk, G. von Plessen, and U. Kreibig, J. Phys. D: Appl. Phys. **37**, 3133 (2004).
[28] B. Palpant, B. Prevel, J. Lerme, E. Cottancin, M. Pellarin, M. Treilleux, A. Perez, J. L. Vialle, and M. Broyer, Phys. Rev. B **57**, 1963 (1998).
[29] M. Z. Quinten, Z. Phys. B: Condens. Matter **101**, 211 (1996).
[30] U. Kreibig, J. Phys. (Paris) **38**, C2 (1977); U. Kreibig, in *Growth and Properties of Metal Clusters*, edited by J. Bourdon (Elsevier, Amsterdam, 1980), p. 371.
[31] T. Yamaguchi, M. Ogawa, H. Takahashi, and N. Saito, Surf. Sci. **129**, 232 (1983).
[32] X. Qian and H. S. Park, J. Mech. Phys. Solids **58**, 330 (2010).
[33] D. Werner, S. Hashimoto, and T. Uwada, Langmuir **26**, 9956 (2010).
[34] S. K. Mandal, R. K. Roy, and A. K. Pal, J. Phys. D **35**, 2198 (2002).
[35] S. K. Ghosh, S. Nath, S. Kunda, K. Esumi, and T. Pal, J. Phys. Chem. B **108**, 13963 (2004).
[36] C. Weiping and Z. Lide, J. Phys.: Condens. Matter **9**, 7257 (1997).
[37] T. Yamaguchi, S. Zoshida, and A. Kinbara, Thin Solid Films **21**, 173 (1974).
[38] V. Resta, C. N. Afonso, E. Piscopiello, and G. Van Tendeloo, Phys. Rev. B **79**, 235409 (2009).
[39] H. Hovel, S. Fritz, A. Hilger, and U. Kreibig, Phys. Rev. B **48**, 18178 (1993).
[40] K. C. Vernon, A. M. Funston, C. Novo, D. E. Gomez, P. Mulvaney, and T. J. Davis, Nano Lett. **10**, 2080 (2010).
[41] D. E. Aspnes, A. A. Studna, and E. Kinsbron, Phys. Rev. B **29**, 768 (1984).
[42] M. M. Giangregorio, M. Losurdo, A. Sachetti, P. Capezzuto, and G. Bruno, J. Lumin. **121**, 322 (2006).
[43] M. Losurdo, M. Bergmair, G. Bruno, D. Cattelan, C. Cobet, A. de Martino, K. Fleischer, Z. Dohcevic-Mitrovic, N. Esser, M. Galliet, R. Gajic, D. Hemzal, K. Hingerl, J. Humlicek, R. Ossikovski, Z. V. Popovic, and O. Saxl, J. Nanopart. Res. **11**, 1521 (2009).
[44] D. E. Aspnes and J. B. Theeten, J. Appl. Phys. **50**, 4928 (1979).
[45] E. Hauser, R. J. Zirke, J. Tauc, J. J. Hauser, and S. R. Nagel, Phys. Rev. Lett. **40**, 1733 (1978).
[46] D. A. G. Bruggeman, Ann. Phys. **24**, 636 (1935).
[47] Z. Ma and L. H. Allen, Phys. Rev. B **48**, 15484 (1993).
[48] D. E. Aspnes, E. Kinsbron, and D. D. Bacon, Phys. Rev. B **21**, 3290 (1980).
[49] C.-L. Kuo and P. Clancy, Surf. Sci. **551**, 39 (2004).
[50] G. Yin, S. Y. Wang, M. Xu, and L. Y. Chen, J. Korean Phys. Soc. **49**, 2108 (2006).
[51] S. Link and M. A. El-Sayed, J. Phys. Chem. B **103**, 8410 (1999).
[52] D. M. Schaadt, B. Feng, and E. T. Yu, Appl. Phys. Lett. **86**, 063106 (2005).
[53] R. Gupta, M. J. Dyer, and W. A. Weimer, J. Appl. Phys. **92**, 5264 (2002).
[54] P. B. Johnson and R. W. Christy, Phys. Rev. B **6**, 4370 (1972).
[55] G. B. Pells and M. Shiga, J. Phys. C **2**, 1835 (1969).
[56] C. Sönnichsen, T. Franzl, T. Wilk, G. von Plessen, J. Feldmann, O. Wilson, and P. Mulvaney, Phys. Rev. Lett. **88**, 077402 (2002).
[57] S. Link and M. A. El-Sayed, J. Phys. Chem. B **103**, 4212 (1999).